

Magnetization-reversal processes in an ultrathin Co/Au film

J. Ferré, V. Grolier, P. Meyer, and S. Lemerle

Laboratoire de Physique des Solides, associé au CNRS, Bât. 510, Université Paris-Sud, 91405 Orsay, France

A. Maziewski, E. Stefanowicz, S. V. Tarasenko, V. V. Tarasenko, and M. Kisielewski

Institute of Physics, Warsaw University Branch, 15 424 Białystok, Lipowa 41, Poland

D. Renard

IOTA, associée au CNRS, Bât. 503, Université Paris-Sud, 91405 Orsay, France

(Received 31 May 1996)

Magnetization-reversal processes in a ferromagnetic cobalt film structure (Au/Co/Au), with perpendicular anisotropy, were investigated by magneto-optical magnetometry and microscopy. In the considered ultrathin Co film, the magnetization reversal between the two Ising-spin equilibrium states is dominated by the domain-wall motion mechanism. We focused our studies on processes initiated from a given demagnetized state. Starting from a magnetically saturated state generated under a large field H_S , applied perpendicular to the film, this demagnetized state is created through magnetic aftereffects in a field H_d antiparallel but smaller than H_S and applied during a selected time. Direct (R^D) and indirect (R^I) magnetization processes are then studied from this state for application of the field parallel and antiparallel to H_d , respectively. The dynamics of the magnetization reversal is much faster for the R^I process since it is initiated from a quasihomogeneous "Swiss cheese" domain state with small nonreversed regions. The magnetic accommodation phenomenon is studied, and a domain-shape memory effect evidenced. A theoretical analysis of the dynamics of magnetization processes is proposed, starting from the model of a patchy inhomogeneous media with a realistic distribution of local coercivities. The pertinent parameters for calculations are deduced from our experimental data using appropriate analytical expressions of the magnetic relaxation time and domain-wall velocity under a field. Computer simulations using these parameters reproduce well the time evolution of the magnetic domain pattern and different magnetization curves both for R^D and R^I magnetization processes. [S0163-1829(97)02122-X]

I. INTRODUCTION

Ultrathin metallic magnetic films stand as model systems for investigating magnetism in two dimensions and studying the important role of interfaces. New preparation methods under ultrahigh vacuum enable us to grow ultrathin-film structures of high quality with sharp interfaces. This enabled recently the performance of fundamental studies on the magnetic moment interface enhancement, the role of the surface magnetic anisotropy, and phase transitions¹ and the engineering of materials exhibiting new exciting properties for applications.

Dynamic effects control magnetization reversal in ultrathin magnetic films with perpendicular anisotropy.² Nano-scale crystallographic inhomogeneities or defects have a strong influence on the magnetic domain shape and on the magnetization-reversal dynamics. The aim of the present study is to report on perpendicular-field-induced magnetization reversal in a gold-sandwiched ultrathin Co film and to give a spatial and temporal description of the switching process supported by realistic computer simulations. Ultrathin Co layers ($t_{\text{Co}}=8 \text{ \AA}$) with weak surface roughness guarantee a perpendicular magnetic anisotropy³ and magnetization reversal through domain-wall motion.⁴

Let us recall that domains of micrometric size have already been observed by scanning electron microscopy with polarization analysis in virgin ultrathin cobalt films deposited

on Au(111).^{5,6} By Faraday microscopy a metastable micrometric magnetic domain structure has previously been evidenced in Au/Co/Au(111) sandwiches during magnetization reversal in a magnetic field.² The magnetization reversal dynamics in the considered sample may be successfully explained assuming domain-wall pinning at the boundaries of natural patches, related to the nanocrystalline structure of the Co layer, or at the limit of atomically flat Co terraces.^{3,4,7} Then one has to consider some distribution of the exchange interaction between patches and of the anisotropy depending upon the patch thickness.³ This consequently provides a distribution of local coercivities which affects the magnetization-reversal process. For example, starting from a demagnetized state obtained from a magnetically saturated sample after applying a field perpendicular to the film plane, an asymmetry between magnetization processes induced by "up-" or "down-"oriented fields has been recently observed in Au/Co/Au.⁸

A detailed study of the magnetization-reversal phenomenon, based on domain imaging and magnetic aftereffect experiments in Au/Co/Au sandwiches, is presented, discussed, and compared to simulations. In Sec. II, we describe the main properties of the considered sample and our experimental setup. The results concerning domains and magnetization-reversal dynamics starting from a well-defined demagnetized state are reported in Sec. III. Simulations on the domain dynamics are presented and compared to experimental results

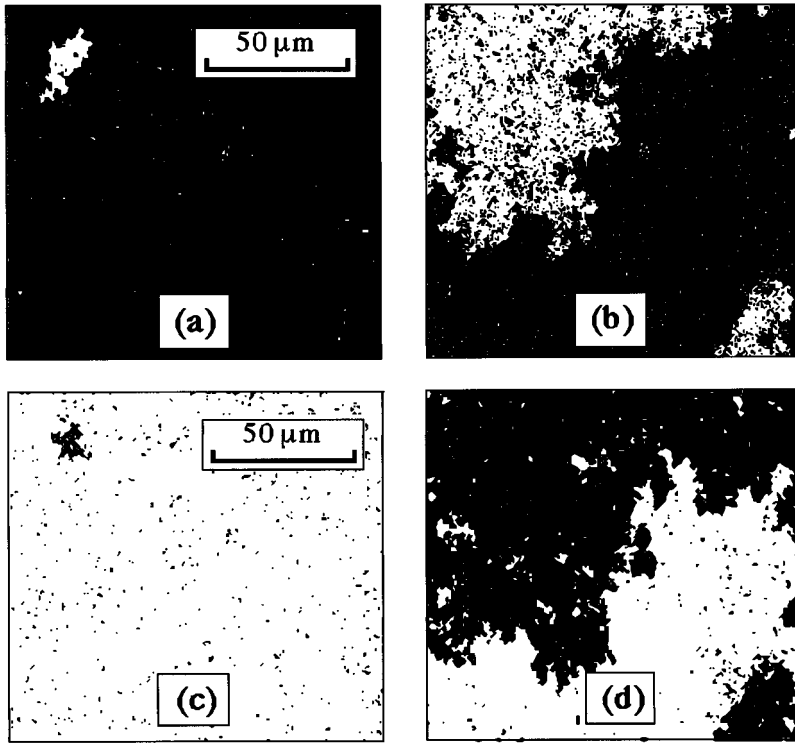


FIG. 1. Starting from a spin-down (in black) or spin-up (in white) saturated state, the application of a positive (a), (b) or negative field H_d (c), (d), respectively, induces first a reversed-magnetized nucleation center. The spin-up or spin-down domain nucleation is well localized in the upper left corner of the images (a) and (c), as shown here after applying a positive or a negative field $H_d = \pm 720$ Oe during $t = 1$ s. Leaving the same positive (b) or negative (d) applied field, a domain structure develops from the nucleation center. The patterns (b) and (d) are then shown after $t = 8$ s.

in Sec. IV. A general discussion and some conclusions follow in Sec. V.

II. SAMPLE AND EXPERIMENTAL SETUP

The preparation and structural properties of Au/Co/Au sandwiches, grown on a glass substrate, have been reported in previous papers.^{9,10} The present magneto-optical investigations are performed on a Au(250 Å)/Co(8 Å)/Au(50 Å) sandwich. The Co film is grown on 250-Å-thick fcc Au(111) buffer layer deposited on float glass. After annealing, the gold crystallites have a lateral size of about 2000 Å. Their surface consists of atomically flat terraces with a typical size of 250 Å. The cobalt film grows on Au(111) with a polycrystalline hcp (0001) structure, and its c axis is closely oriented perpendicularly to the film surface. The cobalt crystallites are slightly misoriented in the plane from each other by less than 2° and their lateral dimension is about 200 Å, while flat Co atomic terraces extend over 70–100 Å.

Usually, the magnetization-reversal process occurs via the nucleation of small reversed domains followed by the propagation of their domain walls. Nucleation-dominated or wall-propagation-dominated reversal mechanisms can be evidenced, depending on the sample thickness and microstructure.² Our 8-Å-thick Co film is chosen to exhibit the second behavior (Fig. 1). Note that, in our case, a domain nucleates always at the same “magnetically soft” extrinsic center for reversed magnetic fields. Since the nucleation field exceeds the propagation field, such a sample exhibits a very square magnetic hysteresis loop (Fig. 2).

Magneto-optical Faraday magnetometry is used to probe the out-of-plane component of the magnetization over a large sample area of about 1 mm^2 . The magnetic field is always applied perpendicular to the film. These measurements are realized using a modulation technique of the state of polar-

ization of the light.¹¹ A high spatial resolution ($0.5 \mu\text{m}$) Faraday microscope, equipped with a sensitive charge-coupled-device camera and subsequent image processing,¹² allows magnetic domain visualization. We report only on room-temperature measurements.

III. EXPERIMENTAL RESULTS

In real ultrathin magnetic films, all kinds of crystalline defects, such as dislocations and atomic steps, play an important role on the domain structure and wall jaggedness. Therefore the demagnetized ($M=0$) state of a real sample cannot be simply calculated as usual for an ideal film by minimizing the overall exchange and magnetostatic energy. The spatial distribution of local energy minima related to film defects described above explains well why the magnetic domain structure depends so strongly on the magnetic history of the sample. Consequently, we have to take into account the distribution of local coercivities. In general, large-scale simulations are then necessary for mapping the magnetization in these structures. For example, the magnetization-reversal behavior has been studied at zero temperature in thick films with a disordered patchy lattice.¹³

A. Initial demagnetized state

In our present studies, the demagnetized state is obtained by the following procedure. The sample is first magnetized at full saturation in a field of 4 kOe, larger than the coercive field $H_c = 770$ Oe. A single “spin-up” or “spin-down” domain state is then created. An inverse field $H = |H_d|$ (such as $|H_d| < H_c$) is suddenly applied during a fixed time $t = t_{1/2}$ to reverse exactly half of the magnetization through the magnetic aftereffect mechanism. The field is then switched rapidly to zero in order to freeze the resulting magnetic domain

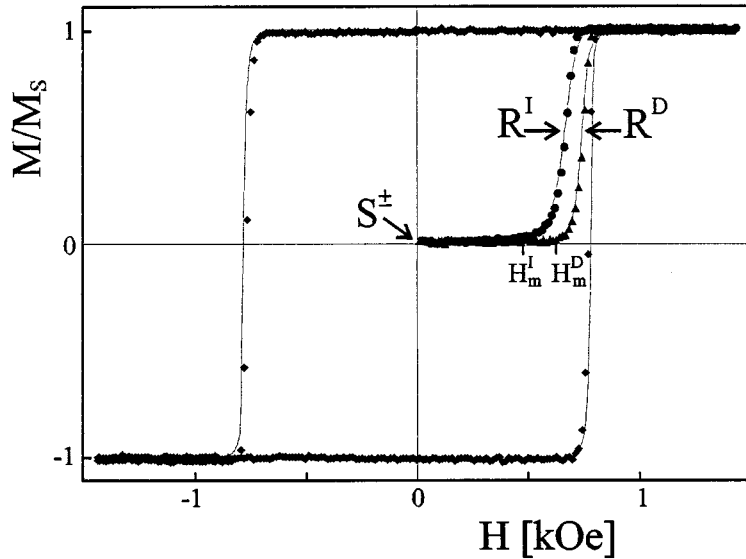


FIG. 2. Magnetic hysteresis loop and initial magnetization curves (direct R^D and indirect R^I processes) measured by Faraday rotation (marks) and numerically simulated (solid lines). The initial S^\pm states are obtained after applying a magnetic field $H_d = \pm 740$ Oe during 10 s on a spin-down or spin-up single-domain state, respectively. The same field-sweeping rate (15 Oe/s) was used for all experiments.

pattern in a demagnetized state with no net magnetization as it can be visualized by magneto-optical microscopy [Figs. 1(b) and 1(d)]. Since this pattern does not evolve during this last procedure, we conclude that the magnetization-reversible process is inefficient for our sample. According to the magnetic aftereffect behavior, a convenient choice of H_d and $t_{1/2}$ allows us to realize easily this demagnetized state. There exists obviously a complete symmetry between the magnetic domain configurations obtained when starting from spin-up or spin-down saturated states and applying negative or positive magnetic fields with the same value during the same time. The demagnetized states generated from either the spin-up (in white) or spin-down (in black) single-domain states (Fig. 1) will be called $S^-(H_d)$ if $H_d < 0$ and $S^+(H_d)$ if $H_d > 0$, respectively.

B. Magnetization mechanisms

Let us consider simple magnetization processes starting from one of the two demagnetized $S^\pm(H_d)$ states. Two distinct cases have to be considered: A ‘‘direct’’ magnetization process R^D corresponds to an applied field H having the same sign as H_d , and an ‘‘indirect’’ process R^I occurs when H is opposite to H_d . The two magnetization curves obtained for R^D and R^I processes starting, for convenience, either from the $S^+(740$ Oe) or $S^-(-740$ Oe) demagnetized states, respectively, and the hysteresis loop measured with the same field sweeping rate are reported in Fig. 2. Up to applied field values $H_m^D = 670$ Oe and $H_m^I = 480$ Oe (both smaller than $H_c = 770$ Oe), respectively for the R^D and R^I procedures, the susceptibility remains vanishingly small, but increases rapidly at higher fields. For the R^D process the field necessary to reach the saturation of the magnetization is close to H_S , determined as usual from the hysteresis loop, while for the R^I process only a smaller field is required.

Let us consider now the dynamics of the direct R^D magnetization process. Starting from a spin-down saturated state, the sudden application of a positive field H_d ($H_d < H_c$) provides the usual time-dependent magnetic aftereffect $M(H_d, t)$ [Fig. 3(a)] which rises up to reach the saturated

spin-up state, consistently with a domain-wall motion dominated mechanism.² The R^D magnetic relaxation in a positive field $H = H_d$, but initiated from the $S^+(H_d)$ demagnetized state, follows exactly the same relaxation law $M(H_d, t)$ as that exhibited in Fig. 3(a) for $t > t_{1/2}(H_d)$. As expected,⁴ the magnetic relaxation is strongly accelerated when increasing the field value, between $H_d = 660$ and 700 Oe [Fig. 3(a)].

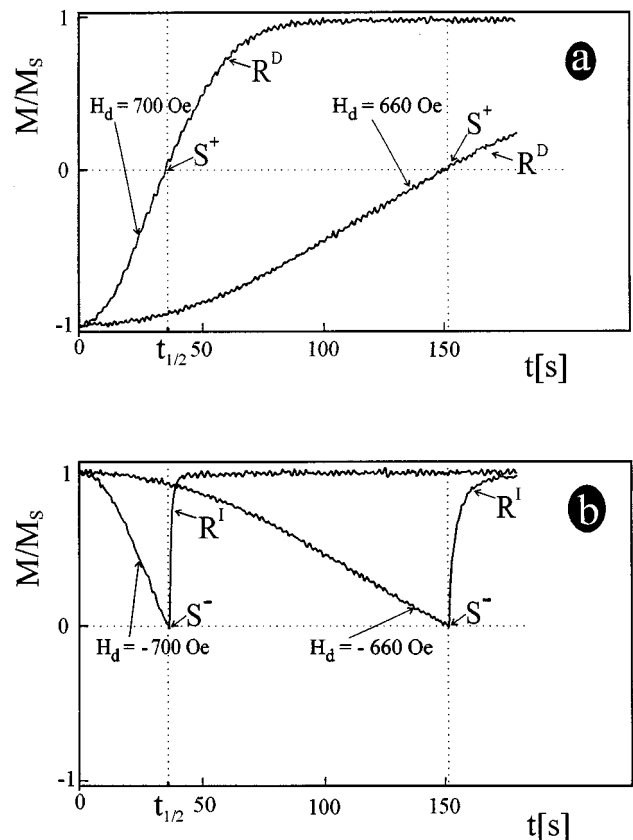


FIG. 3. Dynamics of the (a) $R^D(S^+)$ and (b) $R^I(S^-)$ processes under field $H = \pm |H_d|$, respectively, with $|H_d| = 660$ or 700 Oe. Note the faster magnetic relaxation for the R^I process at the same field value.

Starting now from a spin-up saturated state and applying a reverse field $H_d < 0$, one obviously obtains a symmetric $M(H_d, t)$ relaxation behavior [compare the corresponding curves in Figs. 3(a) and 3(b) for $t < t_{1/2}(H_d)$]. For the R^I process a positive field $H = |H_d|$ is subsequently applied at the demagnetized state, i.e., for $t = t_{1/2}(H_d)$. The dynamics of the R^I magnetization process is much faster [Fig. 3(b)] than for the R^D process at the same field [Fig. 3(a)].

In order to clear up the origin of the magnetization reversal and of such asymmetry in the dynamic behavior, we visualized the evolution of the magnetic domain pattern for the two different D and I procedures. Since the magnetization-reversal process can be stopped for a long time at any moment by switching the field off,² it is easy to visualize the change of the magnetic domain pattern under a given field H as a function of time.

The images of the Figs. 4(a)–4(c) illustrate well the evolution of the magnetic domain structure after applying first a field $H_d = 700$ Oe at time $t = 0$ on a spin-down (in black) single-domain state, which corresponds to the magnetic aftereffect data reported in Fig. 3(a) measured on a larger sample area. As already shown in Fig. 1, after nucleation at time $t = 0$, in a region which is presently located outside from the field of view of our microscope a lacunary spin-up (in white) domain expands by wall motion at the expense of the initial spin-down state. It results in a quasihomogeneous large domain structure in which only small nonreversed spin-down areas are embedded inside the created spin-up magnetized state [Figs. 4(a)–4(c)]. We call this magnetic state a “Swiss cheese” structure. As we shall see later, the existence of remaining nonreversed entities can be explained assuming a distribution of the local coercive force. Such an effect is predicted in inhomogeneous patchy materials for which domains expand by avoiding the hardest magnetic regions. The local magnetization in these last regions switches progressively and disappears (at least at our optical resolution of $0.5 \mu\text{m}$) with elapsed time or when increasing the applied field.

The asymmetry of the magnetization relaxation between the R^D and R^I processes can therefore be investigated by applying an inverse negative field with amplitude $|H| \geq H_m^I$ (Fig. 2). Figures 4(d)–4(f) illustrate the R^I process starting from the nearly demagnetized state $S^+(H_d = 700 \text{ Oe})$ [Fig. 4(c)] and after applying a negative field $H = -550$ Oe with a magnitude smaller than H_d . Such a behavior corresponds to the R^I magnetic relaxation shown above in Fig. 3(b), but recorded here under a weaker applied field in order to slow the dynamics and obtain time-dependent magnetization changes comparable to the direct process. The magnetization reversal occurs through domain-wall motion initiated from a large number of spin-down entities [Figs. 4(d)–4(f)] which act as an assembly of nucleation centers. The considered magnetization-reversal dynamics is obviously accelerated in the R^I process because, first, the sum of the perimeters limiting the spin-down entities by far exceeds the length of the main boundary separating the initial spin-up and spin-down quasihomogeneous states [Fig. 4(c)], and next the magnetization process now takes place at all magnetically softer regions.

Switching the magnetic field again along the positive direction, we still observe [Figs. 4(g) and 4(h)] fast changes of the magnetization due to the expansion of the spin-up phase

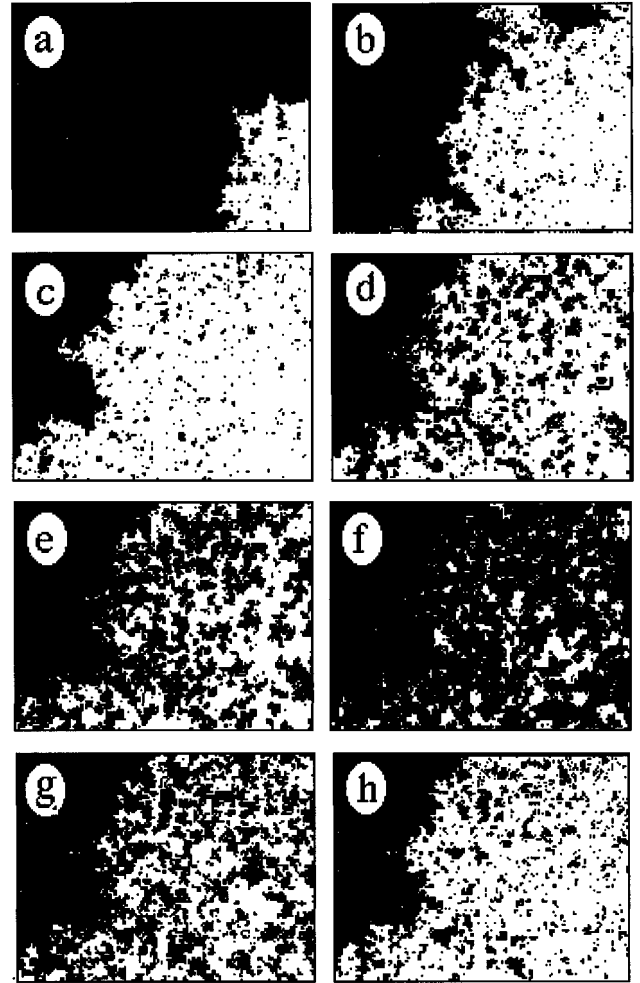


FIG. 4. Time evolution of the magnetic domain structure (image width $150 \mu\text{m}$) starting from an initially saturated spin-down sample (in black) induced by the following sequence of magnetic fields: (i) positive $H_1 = H_d = 700$ Oe [images (a)–(c)] applied during $t_1^+ = 6$ s (a), $t_1^+ = 9$ s (b), and $t_1^+ = 11$ s (c). The direct R^D process is illustrated as the development of a quasihomogeneous spin-up domain (in white). (ii) In order to study the R^I magnetization process starting from the S^- state, the magnetic field was then reversed suddenly. Starting from the state (c), the field is reversed to $H_2 = -550$ Oe and during $t_2^- = 7$ s (d), $t_2^- = 25$ s (e); and $t_2^- = 100$ s (f). (iii) At state (f) a positive $H_3 = |H_2| = 550$ Oe field is applied [images (g) and (h)] during $t_3^+ = 10$ s (g) and $t_3^+ = 100$ s (h). A memory effect is revealed [compare images (c) and (h)].

tending to reconstruct the initial S^+ state [compare Figs. 4(c) and 4(h)]. This phenomenon deals with a domain-structure-shape memory effect due to the fact that the magnetization process goes on, as was mentioned above, in magnetically softer areas.

The magnetic accommodation phenomenon generated from a magnetization procedure starting from the S^- (-740 Oe) demagnetized state (Fig. 5, left) is also studied. Minor magnetization loops resulting from the application of a sequence of alternated rectangular magnetic field pulses with amplitude H [Fig. 5(c)] are recorded. For relatively small field values, $H_m^I < H < H_m^D$, we observe [Fig. 5(a)] that successive magnetization extrema slightly decrease

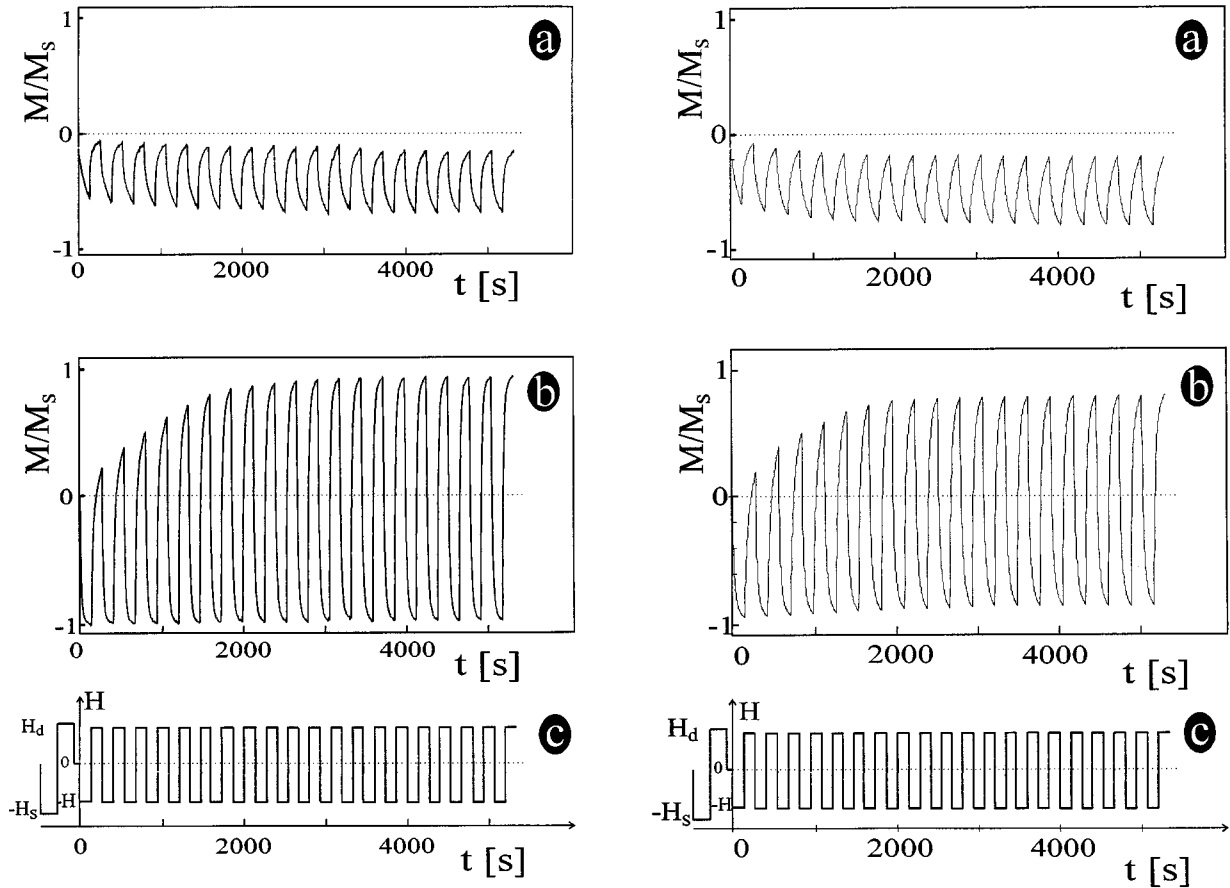


FIG. 5. Magnetic accommodation phenomena [(a),(b)] induced by a sequence of successive rectangular $\pm|H|$ field pulses (c). The measurements are performed starting from the S^- (-740 Oe) demagnetized sample state. Experimental data (left set) and corresponding simulations (right set) in the (a) low- ($H=530$ Oe) and (b) high- ($H=590$ Oe) field regimes.

to stabilize finally at a constant value. At the same time the total amplitude of the oscillations remains nearly constant.

For stronger fields ($H > H_m^D$) [Fig. 5(b)], but smaller than the coercive field (to avoid the saturation of the magnetization), the maximum magnetization value increases progressively with time up to reach a symmetric variation of the magnetization between almost-saturated spin states. Then after applying a strong enough field the Swiss cheese phase spreads over the whole sample area.

IV. THEORETICAL ANALYSIS OF THE MAGNETIZATION PROCESS

A detailed theoretical description of magnetization processes in high-defect-density thin and ultrathin films is limited by some serious mathematical problems. Even a determination of the static distribution of the magnetization in such systems faces many difficulties. The influence of heterogeneity on the magnetization processes in thick films (of about 500 Å) was examined at $T=0$.¹³ Reversal dynamics in ultrathin magnetic films have been recently investigated by computer simulations.¹⁴ Unfortunately, these simulations were done for patchy samples having an homogeneous coercivity which cannot reflect the experimental reality in the present case.

A. Simple description and model choice

To describe our experimental results, we have carried out numerical computer simulations of the magnetization pro-

cesses starting from the knowledge of pertinent physical parameters. These parameters are either deduced from previous experimental data⁴ or extracted from the analytical expressions of observable quantities such as the coercivity and $t_{1/2}$, as presented below. Magnetization processes are dependent upon two mechanisms, namely, the nucleation of domains and the domain-wall motion. In accordance with our presented experimental data (Fig. 1), the thermoactivated nucleation of many centers is negligible at room temperature. We then suppose in the following that the number c of originally created nucleation centers per surface unit does not depend on time at a given field.

Extrapolating previous experimental results,^{4,15} we assume that local domain-wall motion is governed either by a thermally activated pinning mechanism or by viscous motion in an external magnetic field H smaller or higher than the local coercive field H_l , respectively. The local wall velocity v_l may then be expressed as

$$v_l(H) = v_0 \exp[\alpha(H - H_l)] \quad \text{if } H < H_l, \quad (1a)$$

$$v_l(H) = v_0 + \mu(H - H_l) \quad \text{if } H > H_l, \quad (1b)$$

with $\alpha = 2M_s V_p / kT$, where M_s stands for the saturated magnetization. V_p is the activation volume for propagation, k is the Boltzmann constant, and μ is the domain-wall mobility.

The main part of the demagnetizing energy in ultrathin films with large magnetic domains only renormalizes the anisotropy energy.¹⁶ In our model local demagnetizing fields variations are taken into account in the field value H_l .

In order to perform semiquantitative computer simulations, we have to estimate the time scale and space parameters for the investigated magnetization-reversal process from experimental data. As discussed below, the magnetic field dependence of the mean domain-wall velocity v has allowed us to deduce the local coercive field distribution $f(H_l)$ over a wide field region. This distribution satisfies the usual normalization condition

$$\int_0^\infty f(H_l) dH_l = 1. \quad (2)$$

In the low-field regime, only thermally activated stochastic wall motion takes place.¹⁵ Thus, as long as $\bar{H}_{p1} < \int_0^\infty H_l f(H_l) dH_l$ and for $H < 940$ Oe, the mean domain-wall velocity can be written as

$$\begin{aligned} v(H) &= v_0 \int_0^\infty f(H_l) \exp[\alpha(H - H_l)] dH_l \\ &= v_0 \exp[\alpha(H - \bar{H}_{p1})]. \end{aligned} \quad (3)$$

The above conditions are fulfilled in our experimental case, where H is smaller than 750 Oe. In the high-field regime, i.e., for H higher than 1.2 kOe ($H > \bar{H}_{p2}$), we are entirely in the viscous-wall motion regime, so that

$$v(H) = v_0 + \mu \int_0^\infty f(H_l) (H - H_l) dH_l = v_0 + \mu(H - \bar{H}_{p2}). \quad (4)$$

The values of \bar{H}_{p1} and \bar{H}_{p2} were found experimentally to be close to each other.¹⁵ We shall assume $\bar{H}_{p1} = \bar{H}_{p2} = \bar{H}_p$ in the following.

Let us now focus on the low-field stochastic regime ($H < 750$ Oe) in which our domain observations were done. In order to describe the magnetization reversal, it is enough to consider a unit area with periodic boundary conditions containing a single nucleation center (this area is inversely proportional to c , the concentration of nucleation centers). This description is useful for deducing analytical expressions which support numerical simulations of the magnetization processes, as discussed in Sec. IV B. The most convenient way to fulfill periodic boundary conditions is to consider the magnetization reversal of the surface $4\pi R^2 = c^{-1}$ of a ferromagnetic sphere of radius R . Starting from a magnetically saturated sphere at $t=0$, the magnetic-field-induced domain-wall motion causes the demagnetization of a fraction area $\psi(t)$ at time t such as

$$\psi(t) = \sin^2 \left[\frac{1}{2R} \int_0^t v(t') dt' \right]. \quad (5)$$

This expression holds for a domain-wall-dominated magnetization-reversal phenomenon initiated from only few nucleation centers, which is the case in the considered $t_{C0} = 8 \text{ \AA}$ thick sample when $H < 0.75\bar{H}_p$.

In a steady field H_d the mean wall velocity is found to be constant so that the $S^{+(-)}$ demagnetized state is realized for $\psi(t) = 0.5$ at a time $t_{1/2}(H_d)$ given by

$$t_{1/2}(H_d) = \frac{\pi R}{2v_0} \exp[\alpha(\bar{H}_p - H_d)]. \quad (6)$$

It is then interesting to relate the coercivity to pertinent parameters, in particular the constant field sweeping rate s used in hysteresis loop measurements. Then, starting from expression (5) and considering that $H = st$, we deduce

$$\begin{aligned} \psi(H) &= \sin^2 \left[\frac{v_0}{2\alpha s R} e^{-\alpha\bar{H}_p} (e^{\alpha H} - 1) \right] \\ &\cong \sin^2 \left[\frac{v_0}{2\alpha s R} e^{\alpha(H - \bar{H}_p)} \right] \\ &= \sin^2 \left[\frac{\pi}{4\alpha s t_{1/2}(H_d)} e^{\alpha(H - H_d)} \right]. \end{aligned} \quad (7)$$

The coercive field value H_c , measured from the hysteresis loop at a fixed field-sweeping rate, is determined when $\psi(H) = 0.5$, i.e.,

$$H_c = \bar{H}_p + \frac{1}{\alpha} \ln \left[\frac{\pi\alpha s R}{2v_0} \right] \quad (8a)$$

or

$$H_c = H_d + \frac{1}{\alpha} \ln[\alpha s t_{1/2}(H_d)]. \quad (8b)$$

As already demonstrated,³ the coercive field varies logarithmically with the field-sweeping rate, but also depends on the nucleation center concentration since $R \sim c^{-1/2}$.

Then the pertinent set of parameters used later in simulations is evaluated from experimental data. The mean domain-wall velocity v was measured over a wide range of magnetic field (Refs. 2 and 4 and Fig. 6) for the $t_{C0} = 8 \text{ \AA}$ thick cobalt film. The $v(H)$ dependence over the two field regimes can be exactly modeled from expressions (3) and (4) only if one consider an asymmetric $f(H_l)$ distribution function. Thus we constructed it from two halves of Gaussian functions with different widths (Fig. 7):

$$f(H_l) = A \begin{cases} \exp \left[- \left(\frac{H_l - H_{\max}}{\Delta H_1} \right)^2 \right] & \text{if } H_l < H_{\max}, \\ \exp \left[- \left(\frac{H_l - H_{\max}}{\Delta H_2} \right)^2 \right] & \text{if } H_l > H_{\max} \end{cases}, \quad (9)$$

where A is a normalization factor. The shape of the $f(H_l)$ distribution function varies from sample to sample and depends only on details of their nanostructure. ΔH_2 gives rise to the high-field tails of the hysteresis loop.

The experimental $v(H)$ variation (Fig. 6) is well fitted by the theoretical curve using the set of parameters $v_0 = 420$ cm/s, $\alpha = 0.035 \text{ Oe}^{-1}$, $\mu = 13.9$ cm/s Oe, H_{\max}

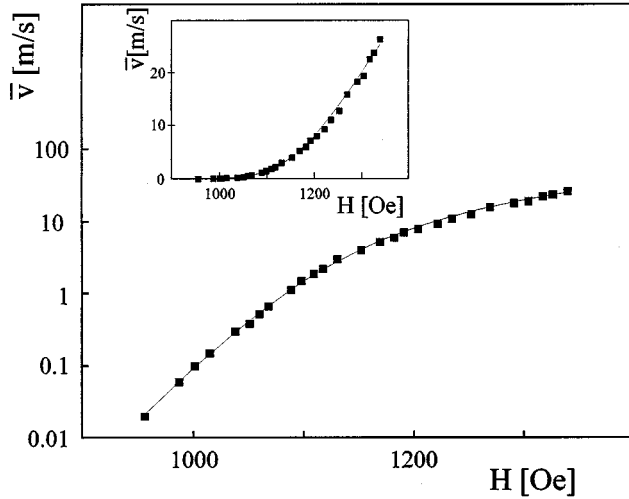


FIG. 6. Domain-wall velocity \bar{v} measured (■) as a function of the applied field H (Ref. 4). The solid curve is a fit with the theoretical function [expression (3)] using parameters values $v_0 = 420 \text{ cm s}^{-1}$, $\alpha = 0.035 \text{ Oe}^{-1}$, $\mu = 14.7 \text{ cm/s Oe}$, and the $f(H_l)$ distribution function [expression (9)] shown in Fig. 7.

$= 1166 \text{ Oe}$, $\Delta H_1 = 86 \text{ Oe}$, and $\Delta H_2 = 125 \text{ Oe}$. The mean propagation field $\bar{H}_p = 1107 \text{ Oe}$ [expression (3)] can be calculated from the knowledge of the $f(H_l)$ function. This means that the viscous regime becomes more efficient than the thermally activated one at fields larger than \bar{H}_p . The fitting errors are estimated to be typically 1% of H_{\max} , a few percent of ΔH_1 , ΔH_2 , and α . Since the available range of high-field values in the pure viscous regime was too limited in our experiments, larger errors up to 40% can be done on v_0 and μ .

An asymmetry of the $f(H_l)$ distribution is needed to fit accurately the $v(H)$ data. There is no reasonable physical basis to assume a symmetric H_l distribution around H_{\max} since it is related to the Co thickness distribution or to the variable exchange interaction between patches. The values of ΔH_1 and ΔH_2 depend drastically on the involved local defects and on the sample preparation conditions.

From the α parameter value the mean activation volume $V_p = 5 \times 10^{-19} \text{ cm}^3$ is estimated. Inserting the values of the parameters v_0 and α and of the calculated \bar{H}_p mean propagation field into expression (6), it is possible to deduce a concentration of nucleation centers $c = 2.1 \times 10^3 \text{ cm}^{-2}$ for the R^D process taking into account that the sample demagnetizes from the saturation state in a time $t_{1/2} = 35.5 \text{ s}$ when applying $H_d = 700 \text{ Oe}$. This value of c is consistent with our experimental observation of fewer than one nucleation center per $1.5 \times 10^{-4} \text{ cm}^2$ area (Fig. 1). We also deduce $H_c = 784 \text{ Oe}$ from expression (8b) for $s = 15 \text{ Oe/s}$, a coercive field which is very close to the experimentally measured value (Fig. 2).

B. Computer modeling and numerical simulations

Computer simulations of the spatial and temporal magnetization-reversal phenomenon have been performed on a (200×200) -cell square lattice. Considering the value of the nucleation centers concentration for the R^D process, we

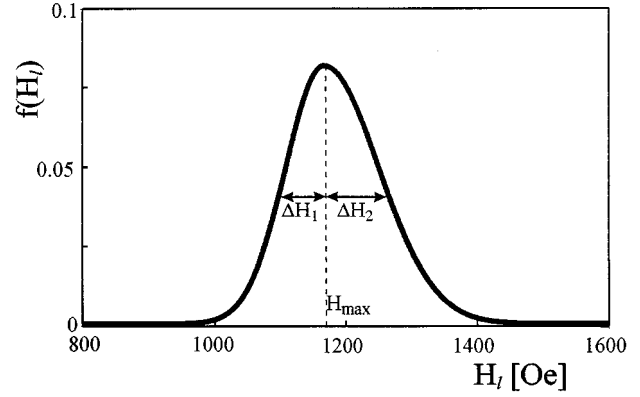


FIG. 7. $f(H_l)$ distribution function of the coercivity used in calculations with parameters $H_{\max} = 1166 \text{ Oe}$, $\Delta H_1 = 86 \text{ Oe}$, and $\Delta H_2 = 125 \text{ Oe}$.

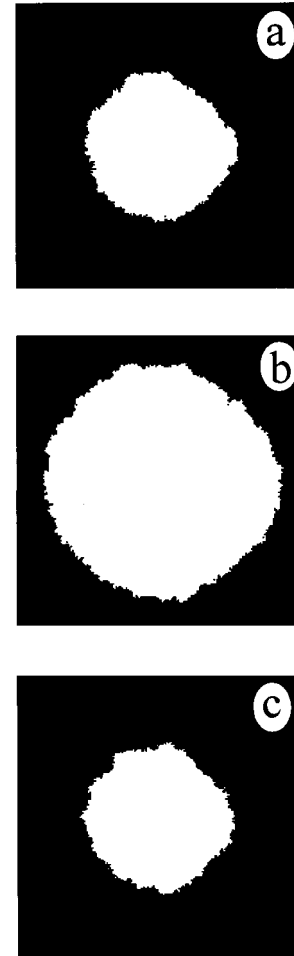


FIG. 8. Simulated domain patterns for an array of identical cells, taking $H_l = \bar{H}_p = 1107 \text{ Oe}$, starting from a saturated spin-down (black) state and applying a field $H_d = 700 \text{ Oe}$. In the R^D process we successively obtain the $M = -0.6M_S$ and demagnetized S^+ state (b). The field is reversed afterwards ($H_d = -700 \text{ Oe}$) to realize a R^I process. The last image (c) presents a restored magnetized $M = -0.6M_S$ state.

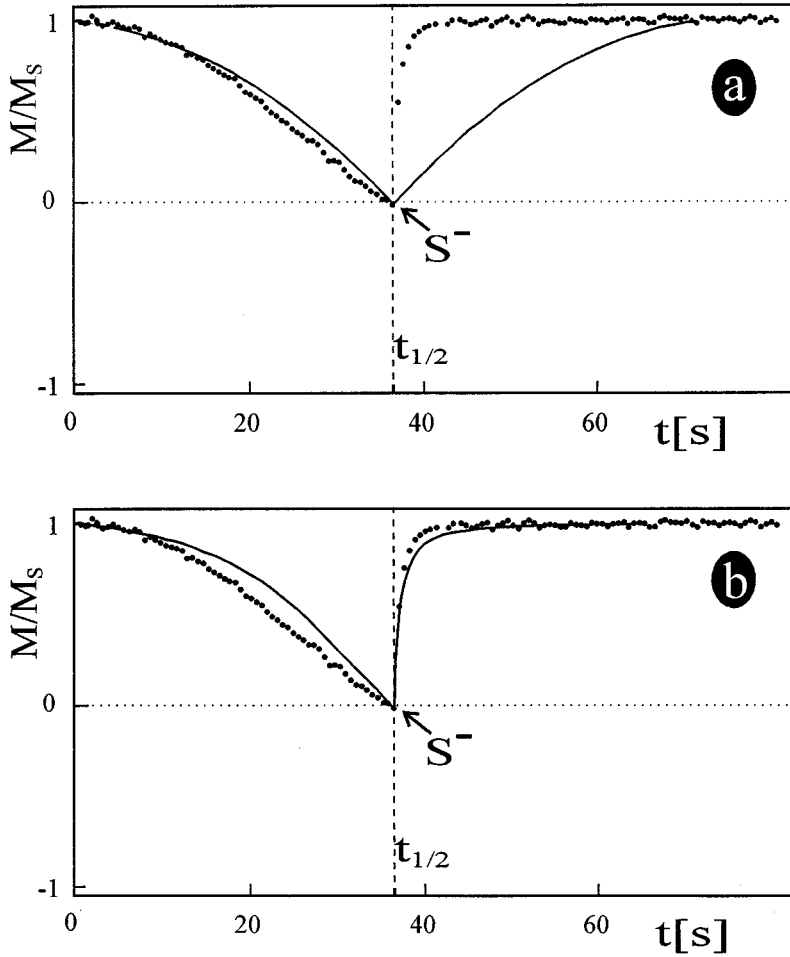


FIG. 9. Simulated magnetization relaxation curves (solid line) under a field $H = \mp 700$ Oe compared with experimental data (\bullet) for (a) an array of identical cells having the same coercivity $H_l = \bar{H}_p = 1107$ Oe; this case corresponds to domain patterns shown in Fig. 8; and (b) a sample characterized by the $f(H_l)$ distribution function of local coercive fields (Fig. 7) randomly distributed in space; this case corresponds to domain patterns presented in Fig. 10.

are able to simulate the magnetization reversal over an $L \times L$ area, where $L = c^{-1/2} = 220 \mu\text{m}$. This leads to a cell length $\delta = 1.1 \mu\text{m}$, which is larger than the elementary propagation length $l_p = (V_p/t_{C0})^{1/2}$ equal to 250 \AA . Thus one assumes that the previously considered local coercive field distribution function $f(H_l)$ is still valid at the micronic scale.

In simulations, we consider that the magnetization reversal by domain-wall motion starts from a spin-reversed nucleation region of 10×10 cells chosen at the center of the lattice. This process is characterized by a switching time τ_p of a cell interacting with its reversed neighbors such as

$$\tau_p(H_l, H) = \Omega \delta / v(H_l, H), \quad (10)$$

where H_l is the local coercive field of a given cell, and $v(H_l, H)$ is given by expressions (1) in the two regimes. The Ω parameter is used to rescale the computer step unit to real time; in a very simple model, it could be equal to L/δ , a ratio equal to 43 in the present case. However, to reproduce well by simulations the experimental aftereffect time $t_{1/2}(H_d = 700 \text{ Oe}) = 35.5 \text{ s}$, we have to fix $\Omega = 8.6$. Considering the huge sensitivity of $t_{1/2}$ with the applied field value, this difference may be accounted by uncertainties on field calibration (of the order of 5%) between imaging [measure of $v(H)$] and magnetic relaxation experiments.

Now let us consider an elementary magnetization-reversal process occurring during a computer step Δt in the neighborhood of a previously switched cell. The reversal process

is first examined in cells ($H_l < \bar{H}$) where the viscous regime occurs; thus, we define τ_{\min} as the shortest time for switching the examined cell over all possible paths. Then the slower stochastic switching regime ($H_l > \bar{H}$) is investigated taking into consideration the surrounding cells. The magnetization-switching probability in these unreversed cells is expressed by

$$P = 1 - \prod_{i=1}^z [1 - \Delta\tau_i / \tau_p], \quad (11)$$

where the product is calculated over all the z neighboring cells and the $\Delta\tau_i$ is defined as (1) the real time Δt of a computer step if the cell has been reversed in former steps, (2) $\Delta\tau_i = 0$ if the cell is not reversed, or (3) $\Delta\tau_i = \Delta t - \tau_{\min}$ if the cell has been reversed in the current simulation step. Note that, since in our domain-imaging experiments (Fig. 4) the applied field is far smaller than \bar{H}_p , only the stochastic domain-wall motion regime is efficient and in this case $\tau_{\min} = 0$.

First of all, we analyze the direct R^D and indirect R^I magnetization processes in the simplest case of an array of identical cells, i.e., when $H_l = \bar{H}_p$ for all l values. Let us start from a single spin-down domain state (in black). The computed evolution of a spin-up domain (in white) in a positive magnetic field H smaller than \bar{H}_p and the related relaxation of the magnetization are presented in Fig. 8 and by the solid

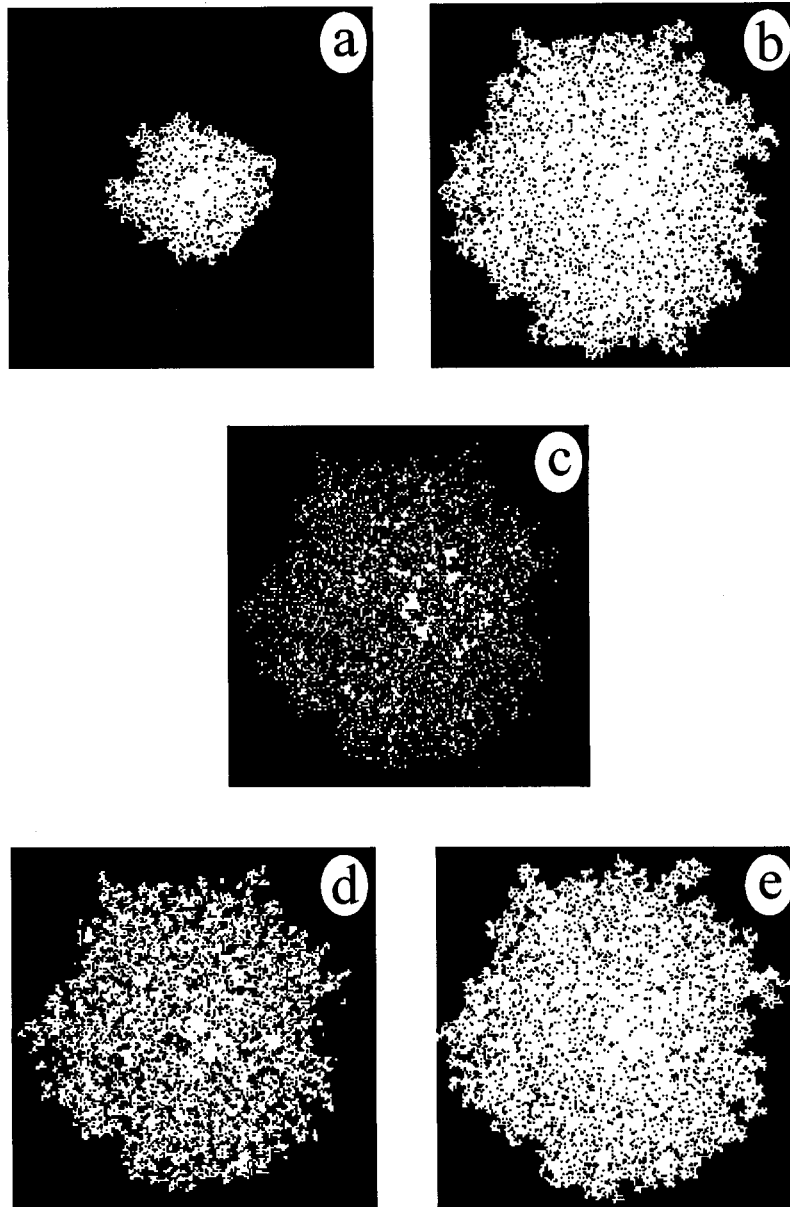


FIG. 10. Simulated evolution of the domain pattern for an array of cells with local coercivity obeying to the $f(H_l)$ distribution function randomly and distributed in space, starting from an initially saturated spin-down (black) state and induced by the following sequence of applied fields: (i) $H_d = +700$ Oe: $M = -0.8M_S$ (a) and demagnetized S^+ (b) states. The growing size of a quasihomogeneous spin-up domain upon the direct R^D process is illustrated. (ii) At state (b) the field is switched to $H = -700$ Oe. The Swiss cheese state (c) ($M = -0.8M_S$) is obtained via the R^I process (iii) At state (c) the field is switched again to $H = +700$ Oe. The images (d) and (e) correspond to $M = -0.4M_S$ and $M = 0$ states, respectively. The memory effect is clearly evidenced by the reconstruction (e) of the initial (b) domain structure.

curve of Fig. 9(a), respectively. As expected, in the pure viscous regime, i.e., when $H > \bar{H}_p$, we obtain a uniform steady motion of the magnetization front. On the simulated images (Fig. 8), for an array of identical cells, we obviously find that the direct R^D and indirect R^I magnetization processes measured at the same field are nearly symmetric with time, as also depicted on the magnetic relaxation (solid curve, Fig. 9). Temporal randomness of domain-wall motion is only responsible in this case for the roughness of the wall boundary (Fig. 8). For the R^I process, we experimentally find that the nonreversed areas of the Swiss cheese domain structure (Fig. 4) grow inside the spin-up state; from simulations,

we show that this behavior is not expected for a sample with uniform coercivity. So the spatial randomness of the local coercive field needs to be considered in real cases for a proper description of the studied magnetization-reversal processes in addition to the temporal randomness.

For a direct comparison between simulation and experimental data, one has to consider that the coercive field H_l of the different cells is distributed in both space and magnitude. A spatial random distribution is then assumed for H_l . This is valid when the spatial correlations between cells are weak. The heterogeneous sample model describes quantitatively well the asymmetry between the relaxation of the magneti-

zation for R^D and R^I processes (solid curve, Fig. 9) as well as the hysteresis loop and initial R^D and R^I magnetization curves (Fig. 2), in particular the experimental values of H_m^I , H_m^D , and H_c at the used field-sweeping rate.

The corresponding simulated domain structures, obtained for $H = 700$ Oe, are shown in Fig. 10. In the R^D process the quasihomogeneous spin-up domain structure looks similar to our experimental observation [Figs. 4(a)–4(c)]. This is true for the domain-wall jaggedness as well as for the existence of remaining nonreversed regions. These phenomena are connected with both stochastic domain-wall motion in a lattice containing small-size magnetically “harder” regions with a larger H_I value. The R^I process, initiated here in a negative field, gives rise to a drastically different behavior. The most crucial difference is that the boundaries of the remagnetized area remain almost at rest, and the spin-down reversal is mainly concentrated inside the spin-up state [compare Fig. 10 and Figs. 4(d)–4(f)] demonstrating that the switching is much more rapid in the Swiss cheese state for the R^I process. This effect is associated with the presence of a large number of effective nucleation centers in the Swiss cheese state for the R^I process. The presence of the domain-shape-memory effect [Fig. 4] is also evidenced by simulations [Figs. 10(d) and 10(e)].

The curves corresponding to the accommodation magnetization processes induced by sequences of successive field pulses were also simulated (Fig. 5, right). The periods of the field pulses are taken according to experimental ones. The qualitative good agreement between simulations and experimental results can be noticed both in small- [Fig. 5(a)] and high- [Fig. 5(b)] field regimes.

V. DISCUSSION AND CONCLUSION

The field-induced magnetization reversal in ultrathin films with perpendicular anisotropy is governed by the magnetic film nanostructure, i.e., the defects localized at the frontier between crystallites, the size of atomically flat terraces, etc.³ In low fields the magnetization reversal is thermally activated. In our Au/Co/Au ultrathin films, the mean size of activation volumes V_p was estimated to be about 250 \AA ,⁴ and results from a balance effect between the cobalt crystallite size (70–100 \AA), the domain-wall width, and the size of flat gold terraces (250 \AA).

As a consequence, the structural defects control the low-field-induced domain structure to a much greater extent than magnetostatic effects, by opposition to the usual situation in thicker films. These defects give rise to a spatial distribution

of local coercive fields. Thus, in a direct R^D process, when the magnetization reversal is dominated by a domain-wall motion mechanism, a quasihomogeneous domain structure is first created. This structure, called the Swiss cheese state, consists of a large magnetized area having inside many small nonreversed entities located at magnetically “harder” regions. The lacunarity of this state is obviously reduced when increasing the duration or magnitude of the applied field. These nonreversed entities act as many nucleation centers when the magnetic field is subsequently reversed (R^I process). Therefore a strong difference in dynamic behavior between direct R^D and indirect R^I magnetization processes can be evidenced on magnetic aftereffect relaxation curves or more directly on the time dependence of the magnetic domain structure. The study of the dynamics of the R^D and R^I processes could be used to determine the coercive field distribution function.

The distribution function of local coercivities can be determined from the experimental field dependence of the domain-wall velocity. Thus the role of sample defects on remagnetization processes may be tested by computer simulations based on the model of a patchy nonhomogeneous film. Simulation results are found to be in good quantitative agreement with experimental data from a spatial and temporal point of view. In particular, the topology of the domain patterns and memory effects are analyzed in the frame of the magnetization-reversal dynamics.

As in thicker films,¹⁷ a direct consequence of a nanoscale distribution of the coercivity is the domain-boundary jaggedness. The domain-wall roughness can be evaluated in our ultrathin Co film by measuring its fractal dimension.⁴ Thus more work has to be done in the future to relate the domain-wall fractality and the domain lacunarity to the applied field and local field distributions.

Our realistic computer simulations could be also applied to explain in details the experimental data obtained on the domain structure and wall jaggedness in thicker TbFeCo films and Co/Pt multilayers,^{17–20} which stand as very promising magneto-optical recording media.

ACKNOWLEDGMENTS

The authors are grateful to M. Galtier for the sample preparation and characterization. We thank Dr. J. P. Jamet, Professor J. Pommier, Dr. A. Stankiewicz, and Professor A. Sukstanski for helpful discussions and comments. This work has been performed in the frame of the European Human Capital and Mobility project Nb. ERB CHRX CT 930316 on “Magnetic properties of novel magnetic structures.”

¹U. Gradmann, in *Handbook of Magnetic Materials*, edited by K. H. J. Buschow (Elsevier Science, New York, 1993), Vol. 7.

²J. Pommier, P. Meyer, G. Pénissard, J. Ferré, P. Bruno, and D. Renard, *Phys. Rev. Lett.* **65**, 2054 (1990).

³P. Bruno, G. Bayreuther, P. Beauvillain, C. Chappert, G. Luggert, D. Renard, J. P. Renard, and J. Seiden, *J. Appl. Phys.* **68**, 5759 (1990).

⁴A. Kirilyuk, J. Ferré, and D. Renard, *Europhys. Lett.* **24**, 403 (1993).

⁵R. Allenspach, M. Stampanoni, and A. Bishof, *Phys. Rev. Lett.* **65**, 3344 (1990).

⁶M. Speckmann, H. P. Oepen, and H. Ibach, *Phys. Rev. Lett.* **75**, 2035 (1995).

⁷J. Ferré, V. Grolier, A. Kirilyuk, J. P. Jamet, and D. Renard, *J. Magn. Soc. Jpn.* **19**, Suppl. S1, 79 (1995).

⁸A. Maziewski, E. Stefanowicz, V. Tarasenko, V. Grolier, J. Ferré, and D. Renard, *J. Magn. Mater.* **140**, 685 (1995).

⁹D. Renard and G. Nihoul, *Philos. Mag. B* **55**, 75 (1987).

- ¹⁰C. Cesari, J. P. Faure, G. Nihoul, K. Le Dang, P. Veillet, and D. Renard, *J. Magn. Magn. Mater.* **78**, 296 (1989).
- ¹¹V. Grolier, J. Ferré, A. Maziewski, E. Stefanowicz, and D. Renard, *J. Appl. Phys.* **73**, 5939 (1993).
- ¹²P. Meyer, J. Pommier, and J. Ferré, *Proc. SPIE, Int. Soc. Opt. Eng.* **1126**, 93 (1989).
- ¹³H. Fu, R. Giles, M. Mansuripur, and G. Patterson, *Comput. Phys.* **6**, 610 (1992).
- ¹⁴R. D. Kirby, J. X. Shen, R. J. Hardy, and D. J. Sellmyer, *Phys. Rev. B* **49**, 10 810 (1994).
- ¹⁵A. Kirilyuk, J. Ferré, V. Grolier, J. P. Jamet, and D. Renard, *J. Magn. Magn. Mater.* (to be published).
- ¹⁶A. Maziewski, E. Stefanowicz, V. V. Tarasenko, and S. V. Tarasenko (unpublished).
- ¹⁷S. N. Gadetsky, A. V. Stupnov, M. V. Zumkin, and E. N. Nikolaev, *IEEE Trans. Magn.* **28**, 2928 (1992).
- ¹⁸B. E. Bernacki, Te-ho Wu, and M. Mansuripur, *J. Appl. Phys.* **73**, 6838 (1993).
- ¹⁹B. E. Bernacki and M. Mansuripur, *J. Appl. Phys.* **69**, 4960 (1991).
- ²⁰Te-ho Wu and M. Mansuripur, *J. Magn. Soc. Jpn.* **17**, Suppl. S1, 131 (1993).